Eur. Phys. J. C 42, 425–436 (2005)
Digital Object Identifier (DOI) 10.1140/epjc/s2005-02337-3

THE EUROPEAN PHYSICAL JOURNAL C

# Associated production of a light Higgs boson and a chargino pair in the MSSM at linear colliders

G. Ferrera[1,2,a], B. Mele[2,1,b]

[1] Dip. di Fisica, Università La Sapienza, P.le A. Moro 2, 00185 Rome, Italy
[2] Istituto Nazionale di Fisica Nucleare, Sezione di Roma, Rome, Italy

Received: 24 June 2004 / Revised version: 13 May 2005 /
Published online: 19 July 2005 – 

**Abstract.** In the minimal supersymmetric standard model (MSSM), we study the light Higgs boson radiation off a light-chargino pair in the process $e^+e^- \to h\tilde{\chi}_1^+\tilde{\chi}_1^-$ at linear colliders with $\sqrt{s} = 500\,\mathrm{GeV}$. We analyze cross sections in the regions of the MSSM parameter space where the process $e^+e^- \to h\tilde{\chi}_1^+\tilde{\chi}_1^-$ cannot proceed via on-shell production and subsequent decay of either heavier charginos or the pseudoscalar Higgs boson $A$. Cross sections up to a few fb are allowed, according to present experimental limits on the Higgs boson, chargino and sneutrino masses. We also show how a measurement of the $e^+e^- \to h\tilde{\chi}_1^+\tilde{\chi}_1^-$ production rate could provide a determination of the Higgs boson couplings to charginos.

## 1 Introduction

Linear colliders would be a fantastic *precision instrument* for Higgs boson physics and physics beyond the standard model (SM) that could show up at the LHC. In particular, if supersymmetry (SUSY) exists with partners of known particles with masses not too far from present experimental limits, a next-generation linear collider such as the International Linear Collider (ILC) [1] would be able to measure (sometimes with excellent precision) a number of crucial parameters (such as masses, couplings and mixing angles), and eventually test the fine structure of a particular SUSY model. For instance, a linear collider at $\sqrt{s} = 350$–$500\,\mathrm{GeV}$ will be able to disentangle the characteristic two-doublet nature of a light Higgs boson [2] of the minimal supersymmetric standard model (MSSM) [3–5] even in the *decoupling* limit, where the light Higgs mimics the SM Higgs behavior, and all the other Higgs bosons and SUSY partners are out of reach of both the LHC and linear colliders.

Quite a few studies have been carried out to establish the linear-collider potential in determining Higgs boson couplings to fermions, vector bosons, and also to SUSY partners [1]. For coupling *suppressed* by the relatively light mass of the coupled particle (as for the light fermions couplings to the Higgs bosons, where $g_{hf\bar{f}} \sim m_f/v$), the coupling is generally determined through the corresponding Higgs decay branching ratio measurement.

On the other hand, since the main Higgs production mechanisms occur through the *unsuppressed* Higgs boson couplings to vector bosons, the analysis of the Higgs boson production cross sections is expected to provide a good determination of the Higgs bosons couplings to the $Z$ and $W$ vector bosons.

Then, there are a number of couplings of the Higgs bosons to quite heavy particles, other than gauge bosons, that cannot be investigated through Higgs boson decay channels due to phase-space restrictions. In the latter case, the associated production of a Higgs boson and a pair of the heavy particles, when allowed by phase space, can provide an alternative to measure the corresponding coupling. Some reduction in the rate due to the possible phase-space saturation by the heaviness of the final states is expected in this case.

For instance, the SM Higgs boson *unsuppressed* coupling to the top quark, $m_t/v$, can be determined at linear colliders with $\sqrt{s} \sim 1\,\mathrm{TeV}$ through the production rates for the Higgs radiated off a top-quark pair in the channel $e^+e^- \to h\,t\bar{t}$ [6].

The latter strategy can be useful also in the MSSM, that introduces an entire spectrum of relatively heavy partners, that in many cases are coupled to Higgs bosons via an *unsuppressed* coupling constant.

A typical example is that of the light Higgs boson coupling to the light top squark $h\,\tilde{t}_1\tilde{t}_1$, that can be naturally large. The continuum production $e^+e^- \to h\,\tilde{t}_1\tilde{t}_1$ has been studied in [7] as a means of determining this coupling (the corresponding channel at hadron colliders has been investigated also in [8]). Higgs boson production in association with sleptons and light neutralinos in $e^+e^-$ collisions has been considered in [9].

Following a similar strategy, in the present work we want to investigate the possibility to measure the light Higgs coupling to light charginos $h\tilde{\chi}_1^+\tilde{\chi}_1^-$ through the Higgs

[a] e-mail: giancarlo.ferrera@roma1.infn.it
[b] e-mail: barbara.mele@roma1.infn.it

boson production in association with a light-chargino pair at linear colliders,

$$e^+e^- \to h\tilde{\chi}_1^+\tilde{\chi}_1^- \ . \tag{1}$$

Note that *heavy* Higgs bosons couplings to SUSY partners can be mostly explored via Higgs decay rates. For instance, heavy Higgs decays into chargino/neutralino pairs and sfermion pairs in the MSSM have been reviewed in [10]. The *precision* measurement of the Higgs–chargino couplings at a muon collider operating at a heavy Higgs boson resonance has been discussed in [11]. On the other hand, as far as the *light* Higgs boson coupling to light charginos is concerned, not much can be learned through Higgs decay channels due to phase-space restrictions. Indeed, in the MSSM $m_h$ is expected to be lighter that about 130 GeV [12], and the present experimental limit on the chargino mass $m_{\tilde{\chi}_1^+} > 103.5\,\text{GeV}$ (or even the milder one $m_{\tilde{\chi}_1^+} > 92.4\,\text{GeV}$, in case of an almost degenerate chargino and lightest neutralino) [13] excludes the decay $h \to \tilde{\chi}_1^+\tilde{\chi}_1^-$.

Hence, the simplest way to determine the $h\tilde{\chi}_1^+\tilde{\chi}_1^-$ coupling could be through the measurement of the rate for the light Higgs boson production at linear colliders in the channel $e^+e^- \to h\tilde{\chi}_1^+\tilde{\chi}_1^-$. The present mass limits have a good potential for covering a considerable area of the MSSM parameter space, even at $\sqrt{s} \simeq 500\,\text{GeV}$.

We will concentrate on the *non-resonant* continuum production $e^+e^- \to h\tilde{\chi}_1^+\tilde{\chi}_1^-$, that is, we will not include in our study the cases where the considered process proceeds through the on-shell production of either a $\tilde{\chi}_1^+\tilde{\chi}_2^-$ (or the charged conjugated $\tilde{\chi}_1^-\tilde{\chi}_2^+$) or a $hA$ intermediate state (where $\tilde{\chi}_2^-$ is the heavier chargino and $A$ is the pseudoscalar Higgs boson) with a subsequent decay $\tilde{\chi}_2^- \to h\tilde{\chi}_1^-$ and $A \to \tilde{\chi}_1^+\tilde{\chi}_1^-$, respectively. In the latter cases, the total $h\tilde{\chi}_1^+\tilde{\chi}_1^-$ production rates are in general enhanced with respect to the continuum production, that can be viewed as a higher-order process in the electroweak coupling. We will also assume either a low value (i.e., $M_{\tilde{\nu}_e} \simeq 100\,\text{GeV}$) or a quite large value (i.e., $M_{\tilde{\nu}_e} \simeq 500\,\text{GeV}$) for the electron sneutrino mass. The latter suppresses the Feynman diagrams with a sneutrino exchange, involving predominantly the gaugino components of the light charginos.

Note that the SM process $e^+e^- \to HW^+W^-$ (that can be somehow connected by a SUSY transformation to $e^+e^- \to h\tilde{\chi}_1^+\tilde{\chi}_1^-$) has a total cross section of about 5.6 fb for $m_H \simeq 120\,\text{GeV}$, at $\sqrt{s} \simeq 500\,\text{GeV}$ [14].

The measurement of the $h\tilde{\chi}_1^+\tilde{\chi}_1^-$ coupling through the process $e^+e^- \to h\tilde{\chi}_1^+\tilde{\chi}_1^-$ would complement the nice set of precision measurements in the chargino sector expected at future high energy colliders (see [15] and references therein).

The plan of this paper is the following. In Sect. 2, the MSSM parameter regions that are of relevance for the non-resonant $h\tilde{\chi}_1^+\tilde{\chi}_1^-$ production are discussed. We also define three *reference scenarios* for the following analysis. In Sect. 3, the matrix element for $e^+e^- \to h\tilde{\chi}_1^+\tilde{\chi}_1^-$ is presented, and the cross-section computation is described. In Sect. 4, we present total cross sections versus the MSSM parameters. In Sect. 5, we discuss the foreseen sensitivity to a determination of the $h\tilde{\chi}_1^+\tilde{\chi}_1^-$ coupling on an event-number basis, before giving our conclusions in Sect. 6. In Appendix A, we define the interaction Lagrangian and couplings. In Appendix B, we describe the phase-space integration of the relevant squared matrix elements.

## 2 Relevant MSSM parameter space

Charginos are expected to be in general among the lightest SUSY partners in the new particle spectrum of the MSSM. This makes it interesting to consider the production of a light Higgs boson associated to two light charginos in the process $e^+e^- \to h\tilde{\chi}_1^+\tilde{\chi}_1^-$ at $\sqrt{s} = 500\,\text{GeV}$, even if all the particles in the final states are expected to be not so light, and in general heavier than 100 GeV.

Charginos are the mass eigenstates of the mass matrix that mixes charged gaugino and higgsino states (see [4], and Appendix A). At tree level, the latter depends on three parameters, $M_2$, $\mu$ and $\tan\beta$. When the mass matrix is real, the two diagonalizing matrices can be expressed in terms of two mixing angles, $\phi_\pm$. Then, the mass eigenvalues $m_{\tilde{\chi}_1^+}$ and $m_{\tilde{\chi}_2^+}$ and the mixing angles can be analytically written in terms of the parameters $M_2$, $\mu$ and $\tan\beta$. The presence of a Higgs boson in the process $e^+e^- \to h\tilde{\chi}_1^+\tilde{\chi}_1^-$ requires at tree level a further parameter, that can be the pseudoscalar mass $m_{A^0}$. On the other hand, the inclusion of the main radiative corrections to the Higgs boson mass and couplings involves all the basic parameters needed for setting the complete mass spectrum of the SUSY partners in the MSSM. In our study of $e^+e^- \to h\tilde{\chi}_1^+\tilde{\chi}_1^-$ at $\sqrt{s} = 500\,\text{GeV}$, we set $m_{A^0} = 500\,\text{GeV}$. This pushes the pseudoscalar field $A^0$ beyond the threshold for direct production, thus preventing resonant $A^0 \to \tilde{\chi}_1^+\tilde{\chi}_1^-$ contribution to the $h\tilde{\chi}_1^+\tilde{\chi}_1^-$ final state. At the same time, such a large value for $m_{A^0}$ sets a *decoupling-limit* scenario ($m_{A^0} \gg M_Z$).

Present experimental lower limits on $m_h$ [16] in the *decoupling-limit* MSSM are close to the ones derived from the SM Higgs boson direct search (i.e., $m_H > 114.4\,\text{GeV}$ at 95% C.L. [17]).

The corrections to the light Higgs mass and coupling parameter $\alpha$[1] (cf. Appendix A) have been computed according to the code FeynHiggsFast [18], with the following input parameters: $M_{\tilde{t}_{\text{L,R}}} = M_{\tilde{b}_{\text{L,R}}} = M_{\tilde{g}} = 1\,\text{TeV}$, $X_t$ ($\equiv A_t - \mu\cot\beta$) = either 0 or 2 TeV, $A_b = A_t$, $m_t = 175\,\text{GeV}$, $m_b = 4.5\,\text{GeV}$, $\mu = 200\,\text{GeV}$, $M_2 = 400\,\text{GeV}$, and renormalization scale at $m_t$, in the most complete version of the code[2].

Then, in our study, we assumed three different $\tan\beta$ scenarios, and corresponding $m_h$ values for $m_{A^0} = 500\,\text{GeV}$:

[1] The inclusion of radiative corrections to the Higgs boson coupling would require in principle a more general treatment of the complete set of radiative corrections to the process under consideration. On the other hand, one can see that the simple inclusion of the correction to the parameter $\alpha$ is to a good extent self-consistent in our case. The latter has anyway a minor impact on our results.

[2] Varying the $\mu$ and $M_2$ parameters would affect the Higgs spectrum and couplings negligibly.

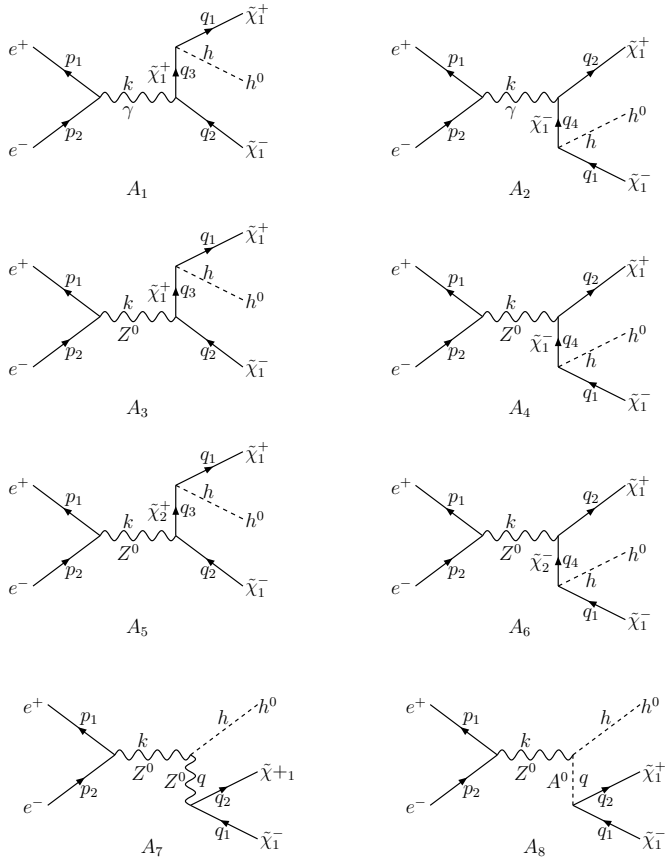


**Fig. 1.** Set of $s$-channel Feynman diagrams contributing to $e^+e^- \to h\tilde{\chi}_1^+\tilde{\chi}_1^-$

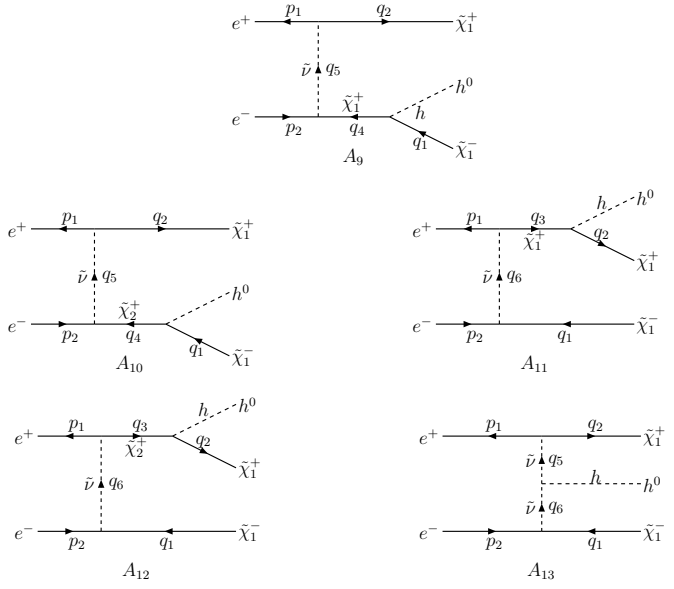


**Fig. 2.** Set of $t$-channel Feynman diagrams contributing to $e^+e^- \to h\tilde{\chi}_1^+\tilde{\chi}_1^-$

(a) $\tan\beta = 3$, with *maximal* stop mixing (i.e., $X_t = 2\,\mathrm{TeV}$), and $m_h = 120.8\,\mathrm{GeV}$;
(b) $\tan\beta = 15$, with *no* stop mixing (i.e., $X_t = 0$), and $m_h = 114.3\,\mathrm{GeV}$;
(c) $\tan\beta = 30$, with *maximal* stop mixing (i.e., $X_t = 2\,\mathrm{TeV}$), and $m_h = 132.0\,\mathrm{GeV}$; these are allowed by present experimental limits [16].

The 13 Feynman diagrams corresponding to the process $e^+e^- \to h\tilde{\chi}_1^+\tilde{\chi}_1^-$ arise either from the $s$-channel $Z^0/\gamma$ exchange (cf. Fig. 1) or from the $t$-channel electron sneutrino $\tilde{\nu}_e$ exchange (cf. Fig. 2). Hence, $M_{\tilde{\nu}_e}$ is a further crucial parameter in the present analysis, influencing the relative importance of $t$-channel diagrams.

In our cross-section evaluation, we include all the 13 diagrams.

In Fig. 3, we show (in either light or dark grey), the area in the $(\mu, M_2)$ plane that is of relevance for the *non-resonant* $e^+e^- \to h\tilde{\chi}_1^+\tilde{\chi}_1^-$ process, for the three different $\tan\beta$ scenarios. The solid lines correspond to the threshold energy contour level:

$$\sqrt{s} = 2\, m_{\tilde{\chi}_1^+} + m_h, \tag{2}$$

while the dashed lines refer to the experimental limit on the light-chargino mass ($m_{\tilde{\chi}_1^+} \simeq 100\,\mathrm{GeV}$).

The straight dot-dashed lines limit from above the region that allows for the associated production of a light chargino $\tilde{\chi}_1^+$ and a resonant heavier chargino $\tilde{\chi}_2^-$ (that we are not interested in), and correspond to

$$\sqrt{s} = m_{\tilde{\chi}_1^+} + m_{\tilde{\chi}_2^-}. \tag{3}$$

A further region of interest (beyond the dark-grey one) is the one where, although $\sqrt{s} > m_{\tilde{\chi}_1^+} + m_{\tilde{\chi}_2^-}$, the heavier chargino is *below* the threshold for a direct decay $\tilde{\chi}_2^+ \to \tilde{\chi}_1^+ h$. Then, again, a resonant $\tilde{\chi}_2^+$ is not allowed. The area where $m_{\tilde{\chi}_2^+} < m_{\tilde{\chi}_1^+} + m_h$ is the one inside the oblique stripes in Fig. 3. The intersection of these stripes with the area between the solid and dashed curves (light-grey regions) is a further region relevant to the non-resonant $e^+e^- \to h\tilde{\chi}_1^+\tilde{\chi}_1^-$ process.

We stress that the constraints on the MSSM parameter space shown in Fig. 3 are purely of a *kinematical* nature.

On the other hand, the dynamical (coupling) characteristics of our process will also derive from the MSSM parameters. For example, it is well known that, in regions where $|\mu| \gg M_2$, the gaugino component in the light charginos is dominant (enhancing the coupling to the sneutrino in the $t$-channel diagrams in Fig. 2), while for $M_2 \gg |\mu|$ light charginos behave mostly like higgsinos (enhancing the couplings to $Z/\gamma$ in the $s$-channel diagrams in Fig. 1).

Since we are particularly interested to a possible determination of the $h\tilde{\chi}_1^+\tilde{\chi}_1^-$ coupling, in Fig. 4 (upper part) we show the behavior of the squared $h\tilde{\chi}_1^+\tilde{\chi}_1^-$ coupling, versus $\mu$, at fixed $M_2$ and $\tan\beta$. In particular, we define

$$\alpha^2_{h\tilde{\chi}_1\tilde{\chi}_1} \equiv |C^{\mathrm{L}}_{11}|^2 + |C^{\mathrm{R}}_{11}|^2 = 2|C^{\mathrm{L}}_{11}|^2\,, \tag{4}$$

where $C^{\mathrm{L,R}}_{ij}$ are defined in Appendix A, by (A.21) and (A.22).

Figure 4 shows clearly that the $h\tilde{\chi}_1^+\tilde{\chi}_1^-$ coupling is maximized for $\mu \simeq M_2$. A second local maximum, that is more pronounced at large $\tan\beta$ values, occurs at $\mu \simeq -M_2$.

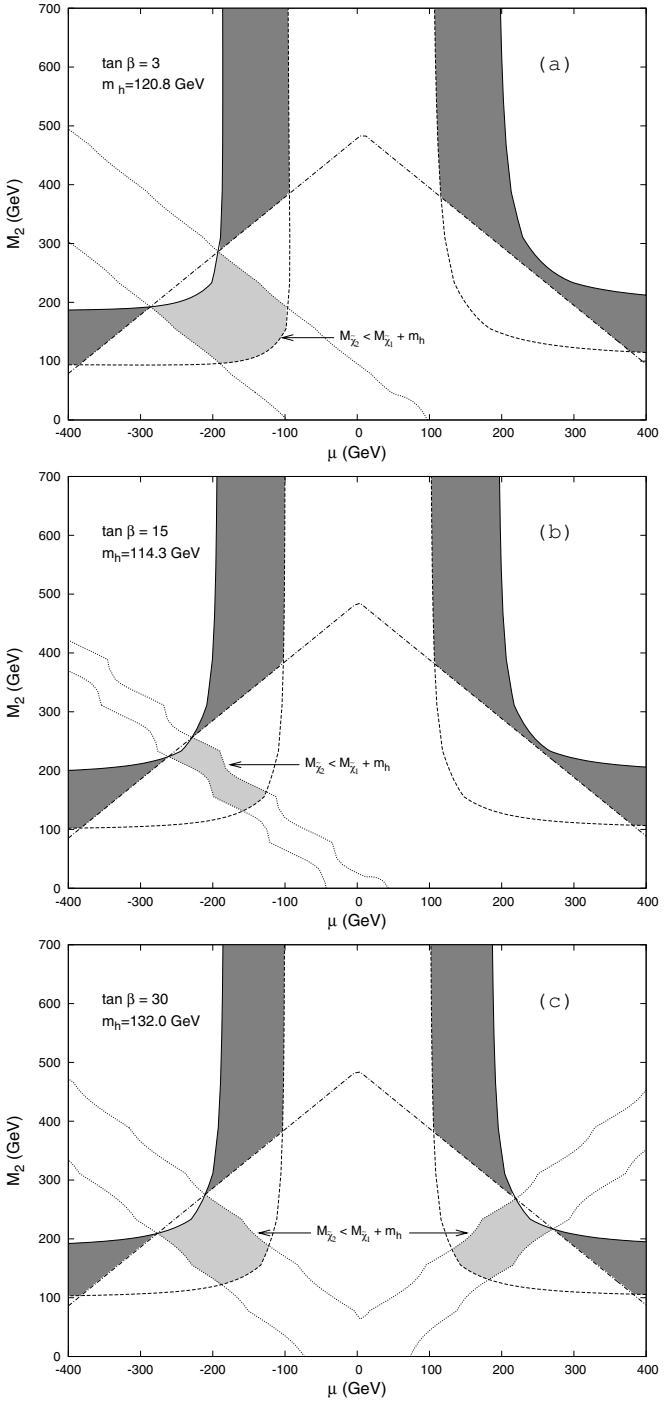


**Fig. 3.** MSSM parameter regions allowed for the continuum production $e^+e^- \to h\tilde{\chi}_1^+\tilde{\chi}_1^-$ at $\sqrt{s} = 500\,\mathrm{GeV}$, for $\tan\beta = 3, 15, 30$ and $m_{A^0} = 500\,\mathrm{GeV}$ (in either light or dark grey)

On the other hand, a ratio $M_2/|\mu|$ quite different from 1 (corresponding to the dominance of either the gaugino or the higgsino component in the $\tilde{\chi}_1^+$) implies in general a depleted $h\tilde{\chi}_1^+\tilde{\chi}_1^-$ coupling. One can then confront the $h\tilde{\chi}_1^+\tilde{\chi}_1^-$ coupling enhancement condition $|\mu| \simeq M_2$ with the allowed parameter space for $e^+e^- \to h\tilde{\chi}_1^+\tilde{\chi}_1^-$ in Fig. 3. The light-grey region (corresponding to $m_{\tilde{\chi}_2^+} < m_{\tilde{\chi}_1^+} + m_h$)

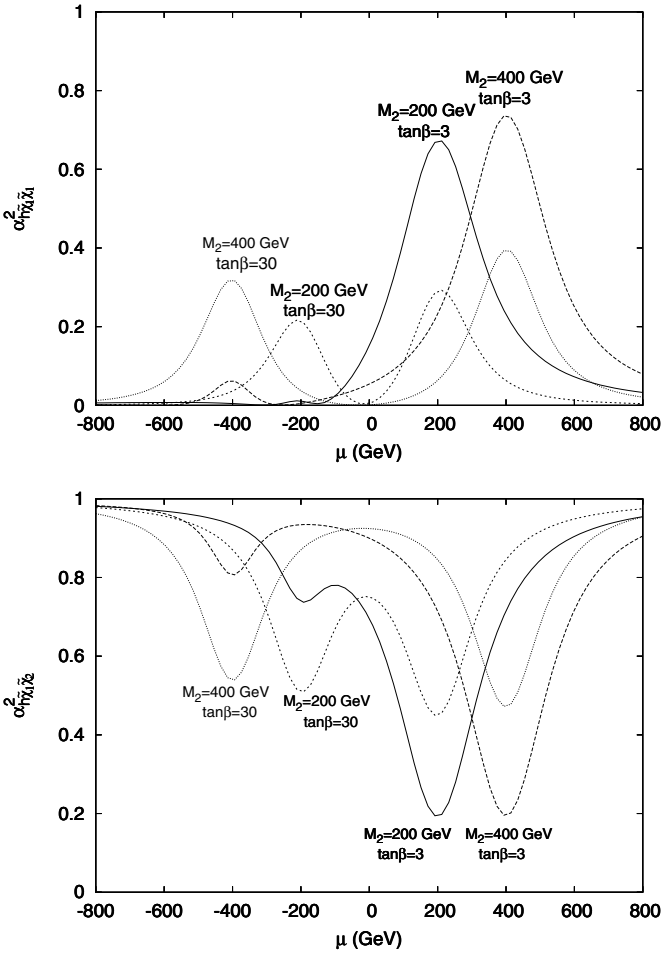


**Fig. 4.** Squared couplings for $h\tilde{\chi}_1^+\tilde{\chi}_1^-$ (upper plot) and $h\tilde{\chi}_1^+\tilde{\chi}_2^-$ (lower plot), as defined by (4) and (5) in the text, respectively

is characterized by a local enhancement of the $h\tilde{\chi}_1^+\tilde{\chi}_1^-$ coupling, that is more pronounced at positive $\mu$ (only allowed at large $\tan\beta$). Instead, in most of the dark-grey region, one has a moderate value of the $h\tilde{\chi}_1^+\tilde{\chi}_1^-$ coupling.

On the other hand, one can note that the parameter dependence of the $h\tilde{\chi}_1^+\tilde{\chi}_2^-$ coupling (entering the amplitudes $A_5, A_6$ in Fig. 1 and $A_{10}, A_{12}$ in Fig. 2), that involves the heavier chargino, is almost complementary to the $h\tilde{\chi}_1^+\tilde{\chi}_1^-$ one. This is clearly shown in the lower part of Fig. 4, where we define

$$\alpha^2_{h\tilde{\chi}_1\tilde{\chi}_2} \equiv |C_{12}^{\mathrm{L}}|^2 + |C_{12}^{\mathrm{R}}|^2 = |C_{21}^{\mathrm{R}}|^2 + |C_{21}^{\mathrm{L}}|^2 \,. \qquad (5)$$

Indeed, the $h\tilde{\chi}_1^+\tilde{\chi}_2^-$ coupling tends to be maximal for most of the parameter values, apart from the regions where $M_2/|\mu| \sim 1$.

The fact that a large $h\tilde{\chi}_1^+\tilde{\chi}_1^-$ coupling implies $M_2/|\mu| \sim 1$ (that is, substantial components of both gaugino and higgsino in the lightest chargino) makes both $s$- and $t$-channel amplitudes relevant for the coupling analysis. This, joined to the complementarity of the $h\tilde{\chi}_1^+\tilde{\chi}_1^-$ and $h\tilde{\chi}_1^+\tilde{\chi}_2^-$ couplings, makes the behavior of the production cross sections for $e^+e^- \to h\tilde{\chi}_1^+\tilde{\chi}_1^-$ in terms of the fundamental MSSM parameters not always easy to interpret.

For this reason, here we study the $h\tilde{\chi}_1^+\tilde{\chi}_1^-$ production rate through a choice of basic parameters differing from the usual one, and affecting the cross-section behavior in a more transparent way. Apart from $\tan\beta$ and the sneutrino mass $M_{\tilde{\nu}_e}$ (the latter mainly influencing the relative importance of $t$-channel amplitudes), we trade the usual parameters $\mu$ and $M_2$ with

(a) the lightest chargino mass $m_{\tilde{\chi}_1^+}$;

(b) the ratio

$$r = \frac{M_2}{|\mu|} \,, \tag{6}$$

and

(c) $\mathrm{sign}(\mu)$.

It will be straightforward to trace back given sets of $(m_{\tilde{\chi}_1^+}, r, \mathrm{sign}(\mu))$ coordinates in the $(\mu, M_2)$ space of the kinematically allowed regions in Fig. 3.

## 3 Cross section evaluation

In this section, we present the $e^+e^- \to h\tilde{\chi}_1^+\tilde{\chi}_1^-$ matrix element. As anticipated in Sect. 2, our analysis includes the complete set of 13 Feynman diagrams presented in Figs. 1 and 2.

The matrix elements corresponding to the amplitudes $A_1, \ldots, A_8$ in Fig. 1 are

$$\begin{aligned}
\mathcal{M}_1 &= \frac{\mathrm{i}ge^2}{k^2+\mathrm{i}\epsilon}\bar{u}^{\chi}_{s_1}(q_1) \\
&\quad\times\left(C^{\mathrm{L}}_{11}P_{\mathrm{L}} + C^{\mathrm{R}}_{11}P_{\mathrm{R}}\right)\frac{(\not{q}_3+M_1)}{q_3^2-M_1^2+\mathrm{i}\epsilon} \\
&\quad\times\gamma^{\mu}v^{\chi}_{s_2}(q_2)\bar{v}^{e}_{r_1}(p_1)\gamma_{\mu}u^{e}_{r_2}(p_2), \\
\mathcal{M}_2 &= \frac{\mathrm{i}ge^2}{k^2+\mathrm{i}\epsilon}\bar{u}^{\chi}_{s_1}(q_1)\gamma^{\mu}\frac{(-\not{q}_4+M_1)}{q_4^2-M_1^2+\mathrm{i}\epsilon} \\
&\quad\times\left(C^{\mathrm{L}}_{11}P_{\mathrm{L}} + C^{\mathrm{R}}_{11}P_{\mathrm{R}}\right)v^{\chi}_{s_2}(q_2)\bar{v}^{e}_{r_1}(p_1)\gamma_{\mu}u^{e}_{r_2}(p_2), \\
\mathcal{M}_3 &= \frac{-\mathrm{i}g^3}{4\cos^2\theta_{\mathrm{W}}(k^2-M_Z^2+\mathrm{i}\epsilon)}\bar{u}^{\chi}_{s_1}(q_1) \\
&\quad\times\left(C^{\mathrm{L}}_{11}P_{\mathrm{L}} + C^{\mathrm{R}}_{11}P_{\mathrm{R}}\right)\frac{(\not{q}_3+M_1)}{q_3^2-M_1^2+\mathrm{i}\epsilon}\gamma^{\mu} \\
&\quad\times\left(O^{\mathrm{L}}_{11}P_{\mathrm{L}} + O^{\mathrm{R}}_{11}P_{\mathrm{R}}\right)v^{\chi}_{s_2}(q_2)\left(g_{\mu\nu}-\frac{k_{\mu}k_{\nu}}{M_Z^2}\right) \\
&\quad\times\bar{v}^{e}_{r_1}(p_1)\gamma^{\nu}(g_V-\gamma_5)u^{e}_{r_2}(p_2), \\
\mathcal{M}_4 &= \frac{-\mathrm{i}g^3}{4\cos^2\theta_{\mathrm{W}}(k^2-M_Z^2+\mathrm{i}\epsilon)}\bar{u}^{\chi}_{s_1}(q_1)\gamma^{\mu} \\
&\quad\times\left(O^{\mathrm{L}}_{11}P_{\mathrm{L}} + O^{\mathrm{R}}_{11}P_{\mathrm{R}}\right)\frac{(-\not{q}_4+M_1)}{q_4^2-M_1^2+\mathrm{i}\epsilon} \\
&\quad\times\left(C^{\mathrm{L}}_{11}P_{\mathrm{L}} + C^{\mathrm{R}}_{11}P_{\mathrm{R}}\right)v^{\chi}_{s_2}(q_2)\left(g_{\mu\nu}-\frac{k_{\mu}k_{\nu}}{M_Z^2}\right) \\
&\quad\times\bar{v}^{e}_{r_1}(p_1)\gamma^{\nu}(g_V-\gamma_5)u^{e}_{r_2}(p_2),
\end{aligned}$$

$$\begin{aligned}
\mathcal{M}_5 &= \frac{-\mathrm{i}g^3}{4\cos^2\theta_{\mathrm{W}}(k^2-M_Z^2+\mathrm{i}\epsilon)}\bar{u}^{\chi}_{s_1}(q_1) \\
&\quad\times\left(C^{\mathrm{L}}_{12}P_{\mathrm{L}} + C^{\mathrm{R}}_{12}P_{\mathrm{R}}\right)\frac{(\not{q}_3+M_2)}{q_3^2-M_2^2+\mathrm{i}\epsilon}\gamma^{\mu} \\
&\quad\times\left(O^{\mathrm{L}}_{21}P_{\mathrm{L}} + O^{\mathrm{R}}_{21}P_{\mathrm{R}}\right)v^{\chi}_{s_2}(q_2)\left(g_{\mu\nu}-\frac{k_{\mu}k_{\nu}}{M_Z^2}\right) \\
&\quad\times\bar{v}^{e}_{r_1}(p_1)\gamma^{\nu}(g_V-\gamma_5)u^{e}_{r_2}(p_2), \\
\mathcal{M}_6 &= \frac{-\mathrm{i}g^3}{4\cos^2\theta_{\mathrm{W}}(k^2-M_Z^2+\mathrm{i}\epsilon)}\bar{u}^{\chi}_{s_1}(q_1)\gamma^{\mu} \\
&\quad\times\left(O^{\mathrm{L}}_{12}P_{\mathrm{L}} + O^{\mathrm{R}}_{12}P_{\mathrm{R}}\right)\frac{(-\not{q}_4+M_2)}{q_4^2-M_2^2+\mathrm{i}\epsilon} \\
&\quad\times\left(C^{\mathrm{L}}_{21}P_{\mathrm{L}} + C^{\mathrm{R}}_{21}P_{\mathrm{R}}\right)v^{\chi}_{s_2}(q_2)\left(g_{\mu\nu}-\frac{k_{\mu}k_{\nu}}{M_Z^2}\right) \\
&\quad\times\bar{v}^{e}_{r_1}(p_1)\gamma^{\nu}(g_V-\gamma_5)u^{e}_{r_2}(p_2), \\
\mathcal{M}_7 &= \frac{\mathrm{i}g^3M_Z\sin(\beta-\alpha)}{4\cos^3\theta_{\mathrm{W}}}\bar{u}^{\chi}_{s_1}(q_1)\gamma^{\mu} \\
&\quad\times\left(O^{\mathrm{L}}_{11}P_{\mathrm{L}} + O^{\mathrm{R}}_{11}P_{\mathrm{R}}\right)v^{\chi}_{s_2}(q_2) \\
&\quad\times\frac{(g_{\mu\nu}-q_{\mu}q_{\nu}/M_Z^2)}{(q^2-M_Z^2+\mathrm{i}\epsilon)}\frac{(g^{\nu\sigma}-k^{\nu}k^{\sigma}/M_Z^2)}{(k^2-M_Z^2+\mathrm{i}\epsilon)} \\
&\quad\times\bar{v}^{e}_{r_1}(p_1)\gamma_{\sigma}(g_V-\gamma_5)u^{e}_{r_2}(p_2), \\
\mathcal{M}_8 &= \frac{\mathrm{i}g^3\cos(\alpha-\beta)}{8\cos^2\theta_{\mathrm{W}}}\bar{u}^{\chi}_{s_1}(q_1) \\
&\quad\times\left(C^{A,\mathrm{L}}_{11}P_{\mathrm{L}} + C^{A,\mathrm{R}}_{11}P_{\mathrm{R}}\right)v^{\chi}_{s_2}(q_2) \\
&\quad\times\frac{(q_{\mu}-h_{\mu})}{(q^2-M_A^2+\mathrm{i}\epsilon)}\frac{(g^{\mu\nu}-k^{\mu}k^{\nu}/M_Z^2)}{(k^2-M_Z^2+\mathrm{i}\epsilon)} \\
&\quad\times\bar{v}^{e}_{r_1}(p_1)\gamma_{\nu}(g_V-\gamma_5)u^{e}_{r_2}(p_2)\,.
\end{aligned} \tag{7}$$

The matrix elements corresponding to the amplitudes $A_9, \ldots, A_{13}$ in Fig. 2 are instead

$$\begin{aligned}
\mathcal{M}_9 &= \frac{\mathrm{i}g^3|V_{11}|^2}{q_5^2-M_{\tilde{\nu}}^2}\bar{v}^{e}_{r_1}(p_1)P_{\mathrm{L}}u^{\chi}_{s_1}(q_1)\bar{v}^{\chi}_{s_2}(q_2) \\
&\quad\times\left(C^{\mathrm{L}}_{11}P_{\mathrm{L}} + C^{\mathrm{R}}_{11}P_{\mathrm{R}}\right)\frac{(-\not{q}_4+M_1)}{q_4^2-M_1^2+\mathrm{i}\epsilon}P_{\mathrm{R}}u^{e}_{r_2}(p_2), \\
\mathcal{M}_{10} &= \frac{\mathrm{i}g^3|V_{11}||V_{21}|}{q_5^2-M_{\tilde{\nu}}^2}\bar{v}^{e}_{r_1}(p_1)P_{\mathrm{L}}u^{\chi}_{s_1}(q_1)\bar{v}^{\chi}_{s_2}(q_2) \\
&\quad\times\left(C^{\mathrm{L}}_{21}P_{\mathrm{L}} + C^{\mathrm{R}}_{21}P_{\mathrm{R}}\right)\frac{(-\not{q}_4+M_2)}{q_4^2-M_2^2+\mathrm{i}\epsilon}P_{\mathrm{R}}u^{e}_{r_2}(p_2), \\
\mathcal{M}_{11} &= \frac{\mathrm{i}g^3|V_{11}|^2}{q_6^2-M_{\tilde{\nu}}^2}\bar{v}^{e}_{r_1}(p_1)P_{\mathrm{L}}\frac{(\not{q}_3+M_1)}{q_3^2-M_1^2+\mathrm{i}\epsilon} \\
&\quad\times\left(C^{\mathrm{L}}_{11}P_{\mathrm{L}} + C^{\mathrm{R}}_{11}P_{\mathrm{R}}\right)u^{\chi}_{s_1}(q_1)\bar{v}^{\chi}_{s_2}(q_2)P_{\mathrm{R}}u^{e}_{r_2}(p_2), \\
\mathcal{M}_{12} &= \frac{\mathrm{i}g^3|V_{11}||V_{21}|}{q_6^2-M_{\tilde{\nu}}^2}\bar{v}^{e}_{r_1}(p_1)P_{\mathrm{L}}\frac{(\not{q}_3+M_2)}{q_3^2-M_2^2+\mathrm{i}\epsilon} \\
&\quad\times\left(C^{\mathrm{L}}_{21}P_{\mathrm{L}} + C^{\mathrm{R}}_{21}P_{\mathrm{R}}\right)u^{\chi}_{s_1}(q_1)\bar{v}^{\chi}_{s_2}(q_2)P_{\mathrm{R}}u^{e}_{r_2}(p_2),
\end{aligned}$$

$$\mathcal{M}_{13} = \frac{\mathrm{i}g^3 M_W \sin(\alpha+\beta)|V_{11}|^2}{2\cos^2\theta_W (q_6^2 - M_{\tilde{\nu}}^2)(q_5^2 - M_{\tilde{\nu}}^2)} \times \bar{v}^e_{r_1}(p_1) P_L u^{\chi}_{s_1}(q_1) \bar{v}^{\chi}_{s_2}(q_2) P_R u^e_{r_2}(p_2) \,. \quad (8)$$

In (7) and (8), we define

$$k = p_1 + p_2 = q_1 + q_2 + h, \quad q_3 = q_1 + h, \quad q_4 = q_2 + h,$$
$$q = p_1 + p_2 - h, \quad q_5 = q_1 - p_1, \quad q_6 = p_2 - q_2$$

and $M_{1,2} = m_{\tilde{\chi}^\pm_{1,2}}$.

All external momenta are defined in Figs. 1 and 2, as flowing from the left to the right, and the different couplings in (7) and (8) are defined in Appendix A. The lower indices of the spinors $u, v$ refer to the particle spin.

We squared, averaged over the initial spin, and summed over the final spin the sum of the matrix elements in (7) and (8) with the help of FORM [19]. Then, one can perform a double analytic integration over the phase-space variables according to the procedure described in Appendix B. This would allow one to obtain an exact *analytic* expression for the Higgs boson momentum distribution:

$$E_h \frac{\mathrm{d}\sigma}{\mathrm{d}^3\mathbf{h}} = \frac{\beta}{s(4\pi)^5} \int_{-1}^{1} \mathrm{d}\cos\vartheta \int_0^{2\pi} \mathrm{d}\varphi \, |\overline{\mathcal{M}}|^2 = f(p_1, p_2, h) \,. \quad (9)$$

The notation is according to Appendix B, and $\mathcal{M} = \sum_{i=1}^{13} \mathcal{M}_i$.

In our computation, we performed instead a completely numerical integration of the squared matrix element in order to obtain total cross sections. The complete code, including the analytic expression of the squared amplitude and the numerical integration routine for the evaluation of the total cross section is available via the authors' e-mail addresses.

In order to check our cross-section computation, we compared our numerical results with the cross sections evaluated by CompHEP [20] on the basis of the same set of Feynman diagrams, and the same input parameters. We found complete agreement by varying the MSSM parameters in the whole relevant range.

## 4 Total cross sections

In Figs. 5 and 6, we show the total cross sections for the process $e^+e^- \to h\tilde{\chi}^+_1\tilde{\chi}^-_1$ at $\sqrt{s} = 500\,\mathrm{GeV}$, in the three scenarios (a), (b), and (c) defined in Sect. 2. Figure 5 assumes a quite light electron sneutrino ($M_{\tilde{\nu}_e} = 100\,\mathrm{GeV}$), while Fig. 6 assumes a heavier sneutrino ($M_{\tilde{\nu}_e} = 500\,\mathrm{GeV}$). Cross sections are shown as functions of $m_{\tilde{\chi}^+_1}$ at different values of the ratio $r = M_2/|\mu|$ (i.e., $r = 1/4, 1/2, 1, 2, 4$). The three plots on the right (left) part of each figure refer to the $\mu > 0$ ($\mu < 0$) case.

In each plot, the allowed range for $m_{\tilde{\chi}^+_1}$ depends on the value of $r$. The variation of this range versus the basic parameters can be easily extrapolated from Fig. 3, keeping in mind that only grey regions in Fig. 3 are kinematically allowed, and that a fixed $r$ value corresponds to a straight line passing through the $M_2 = \mu = 0$ point. To this end, we recall that contours of fixed $m_{\tilde{\chi}^+_1}$ in the parameter space of Fig. 3 are approximate hyperboles, spanning the regions between the two curves referring to $m^{\min}_{\tilde{\chi}^+_1} = 100\,\mathrm{GeV}$ (dashed lines) and $m^{\max}_{\tilde{\chi}^+_1} = (\sqrt{s} - m_h)/2$ (solid lines).

At $r \simeq 1$ and for low and intermediate $\tan\beta$, maximal $m_{\tilde{\chi}^+_1}$ ranges are allowed only for negative $\mu$. At $r = 1/2, 2$, the allowed $m_{\tilde{\chi}^+_1}$ range is always quite reduced by the condition $\sqrt{s} < m_{\tilde{\chi}^+_1} + m_{\tilde{\chi}^-_2}$ (corresponding to the straight dot-dashed lines in Fig. 3), that prevents the resonant production of a heavier chargino.

We can see that, in general, a value $r \simeq 1$ (enhancing amplitudes depending on the $h\tilde{\chi}^+_1\tilde{\chi}^-_1$ coupling) not necessarily corresponds to larger cross sections with respect to the case where $r$ is far from 1. This is mainly due to the competing relevance of the amplitudes involving the $h\tilde{\chi}^+_1\tilde{\chi}^-_2$ coupling. For instance, the dominance of the $r \simeq 2$ cross section on the $r \simeq 1$ cross section for a light $M_{\tilde{\nu}_e}$ [cf. Fig. 5], that is not present for a heavy $M_{\tilde{\nu}_e}$ (cf. Fig. 6), is due to the relative importance of $t$-channel amplitudes involving the heavy chargino (cf. diagrams $A_{10}$ and $A_{12}$ in Fig. 2). Indeed, a value $r > 1$ (i.e., $M_2 > \mu$) tends to increase (decrease) the gaugino component of the heavy (light) chargino.

As a consequence, the sensitivity to the $h\tilde{\chi}^+_1\tilde{\chi}^-_1$ coupling in a measurement of the $e^+e^- \to h\tilde{\chi}^+_1\tilde{\chi}^-_1$ total cross section will very much depend on the actual values of the MSSM parameters, that determine the relative importance of the amplitudes depending on the $h\tilde{\chi}^+_1\tilde{\chi}^-_1$ vertex.

As far as the magnitude of production rates is concerned, for a light sneutrino (cf. Fig. 5) it can reach a few fb even for quite heavy $m_{\tilde{\chi}^+_1}$ ($m_{\tilde{\chi}^+_1} \simeq 150\,\mathrm{GeV}$). The typical production cross section is (not too close to the kinematical saturation of the phase space) of the order of 0.1 fb.

For a heavy sneutrino (cf. Fig. 6), cross sections are in general depleted by an order of magnitude, apart from the case $r \simeq 1$ that, at intermediate and large $\tan\beta$, is quite insensitive to the $M_{\tilde{\nu}_e}$ increase.

Assuming an integrated luminosity of $1\,\mathrm{ab}^{-1}$ at the ILC, the $e^+e^- \to h\tilde{\chi}^+_1\tilde{\chi}^-_1$ event number is expected to be in the range $10 \div 10^3$ for a wide part of the relevant MSSM parameter space.

In the next section, we will discuss the possibility of an experimental determination of the $h\tilde{\chi}^+_1\tilde{\chi}^-_1$ coupling through a measurement of the total event number for $e^+e^- \to h\tilde{\chi}^+_1\tilde{\chi}^-_1$ at $\sqrt{s} = 500\,\mathrm{GeV}$.

## 5 Higgs–chargino coupling determination

In this section, we discuss the potential of a measurement of the total event rate for $e^+e^- \to h\tilde{\chi}^+_1\tilde{\chi}^-_1$ at $\sqrt{s} = 500\,\mathrm{GeV}$ for determining the light Higgs boson coupling to charginos.

Some background for the present reaction is expected from the associated production of a light Higgs and electroweak vector bosons. We do not analyze the background in this paper. We anyhow expect that in the clean environ-

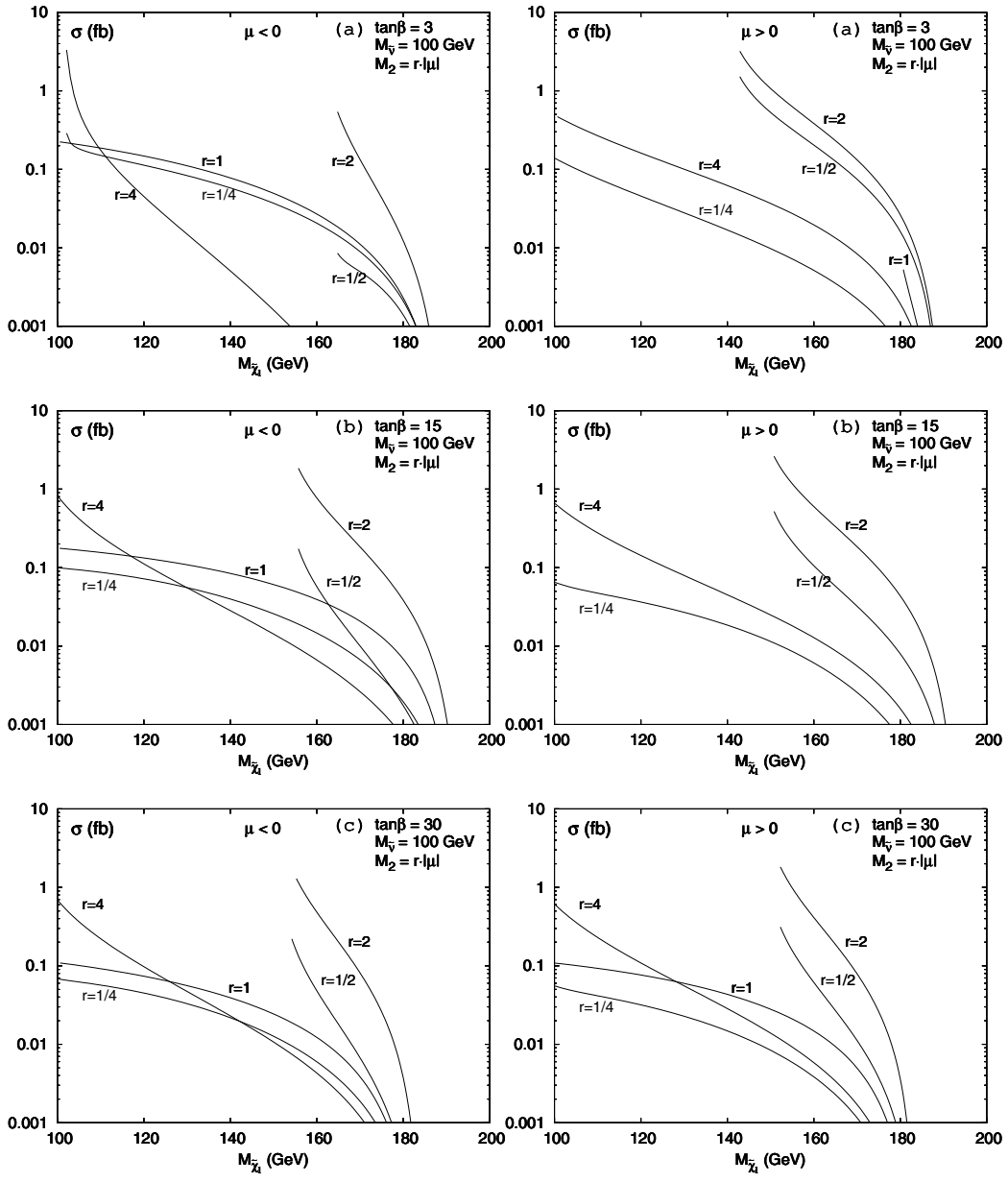


**Fig. 5.** Total cross section for $e^+e^- \to h\tilde{\chi}_1^+\tilde{\chi}_1^-$ at $\sqrt{s} = 500\,\mathrm{GeV}$, for $\tan\beta = 3, 15, 30$, $m_{A^0} = 500\,\mathrm{GeV}$, and $M_{\tilde{\nu}_e} = 100\,\mathrm{GeV}$

ment of $e^+e^-$ collisions the latter will be in general easily distinguishable on the basis of the kinematical characteristics of the final state.

In our analysis we will assume that the precision that can be achieved from a cross-section measurement will be given by the statistical error $\tilde{\sigma}$ on the cross section. For instance, given an integrated luminosity of $1\,\mathrm{ab}^{-1}$ at the ILC, a cross section of 1 (0.1) fb will be affected by a statistical error of $\tilde{\sigma} \simeq 3$ (10)% (corresponding to 1000 (100) events observed).

Our strategy assumes that, before performing the present analysis, all the basic MSSM parameter will have previously been measured through higher-rate supersymmetric particle production processes (typically pair production of supersymmetric partners). Our aim is to check the theoretical consistency of a future experimental determination of the coupling $h\tilde{\chi}_1^+\tilde{\chi}_1^-$ through $e^+e^- \to h\tilde{\chi}_1^+\tilde{\chi}_1^-$, by comparing its value with the MSSM predictions.

In our study, we concentrate on two different frameworks.

The first assumes that the direct decay

$$\tilde{\chi}_2^+ \to \tilde{\chi}_1^+ h$$

is allowed by phase space (dark-grey regions in Fig. 3). Correspondingly, a direct measurement of the $h\tilde{\chi}_1^+\tilde{\chi}_2^-$ coupling will be possible through the $\tilde{\chi}_2^+ \to \tilde{\chi}_1^+ h$ decay rate. We will also assume that the result of this measurement is consistent with the MSSM. Then, we will perform a one-variable analysis of the production rate, by studying the variation of the $e^+e^- \to h\tilde{\chi}_1^+\tilde{\chi}_1^-$ cross section versus a possible change in the $h\tilde{\chi}_1^+\tilde{\chi}_1^-$ coupling with respect to its MSSM value. We quantify the latter change through the parameter $\alpha_1$,

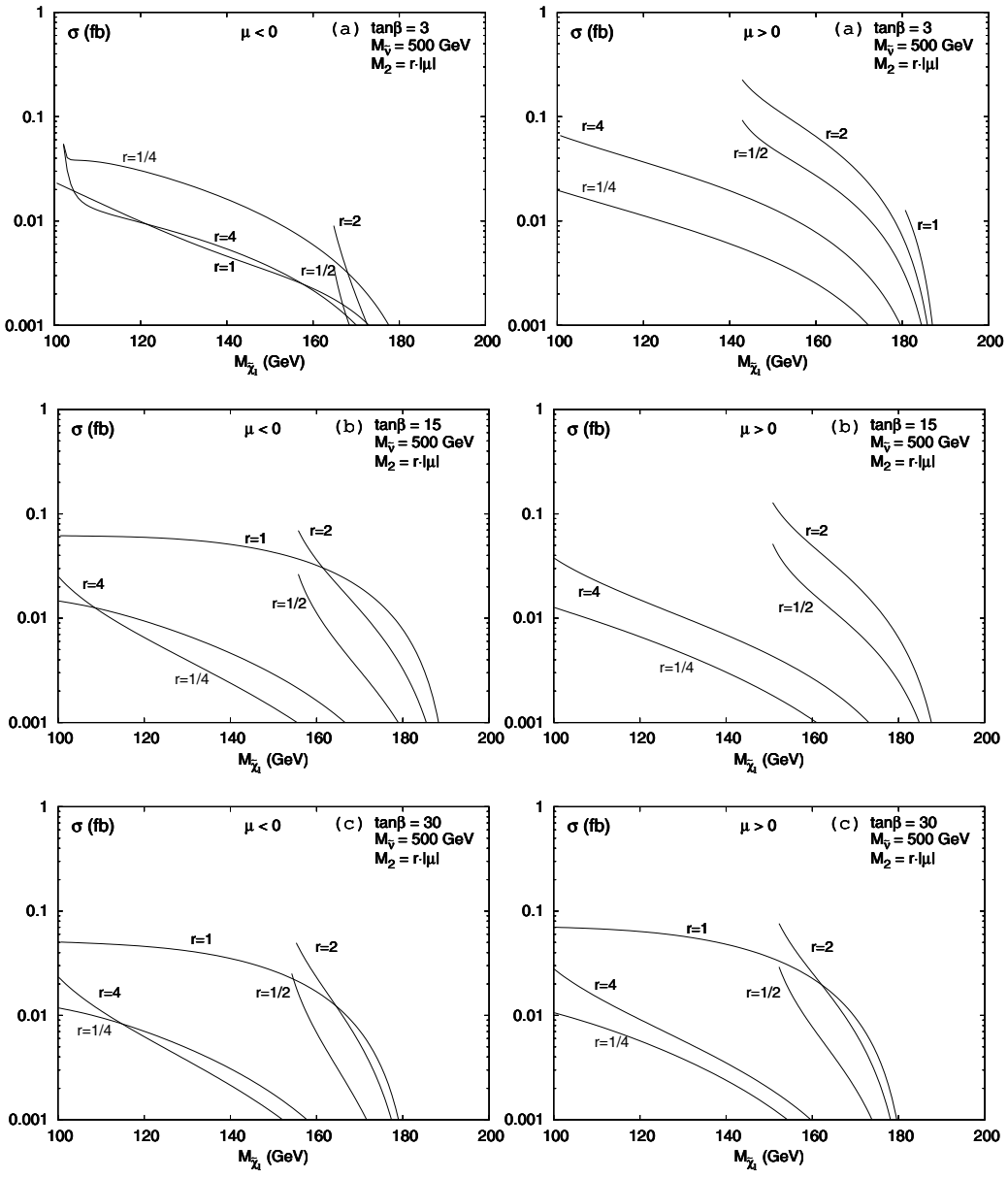


**Fig. 6.** Total cross sections for $e^+e^- \to h\tilde{\chi}_1^+\tilde{\chi}_1^-$ at $\sqrt{s} = 500\,\mathrm{GeV}$, for $\tan\beta = 3, 15, 30$, $m_{A^0} = 500\,\mathrm{GeV}$, and $M_{\tilde{\nu_e}} = 500\,\mathrm{GeV}$

as follows:

$$\mathcal{L}_{h^0\tilde{\chi}_1^+\tilde{\chi}_1^-} \to \alpha_1\, \mathcal{L}_{h^0\tilde{\chi}_1^+\tilde{\chi}_1^-} = \alpha_1\, g\, \overline{\tilde{\chi}}_1(x)\, (C_{11}^{\mathrm{L}} P_{\mathrm{L}} + C_{11}^{\mathrm{R}} P_{\mathrm{R}})\, \tilde{\chi}_1(x)\, h(x)\,. \tag{10}$$

Hence, $\alpha_1$ modifies by a total (real) normalization the $h\tilde{\chi}_1^+\tilde{\chi}_1^-$ coupling in the MSSM Lagrangian (cf. Appendix A).

The second framework assumes that the direct decay

$$\tilde{\chi}_2^+ \to \tilde{\chi}_1^+ h$$

in not allowed by phase space (light-grey regions in Fig. 3). In this case, the $h\tilde{\chi}_1^+\tilde{\chi}_2^-$ coupling (that also enters the $e^+e^- \to h\tilde{\chi}_1^+\tilde{\chi}_1^-$ process) will not be determined through the $\tilde{\chi}_2^+$ decays. Then, we perform a two-variable analysis of the production rate, by introducing a second parameter $\alpha_2$, governing a possible change in the normalization of the $h\tilde{\chi}_1^+\tilde{\chi}_2^-$ coupling

$$\mathcal{L}_{h^0\tilde{\chi}_2^+\tilde{\chi}_1^-} \to \alpha_2\, \mathcal{L}_{h^0\tilde{\chi}_2^+\tilde{\chi}_1^-} = \alpha_2\, g\, \overline{\tilde{\chi}}_1(x)\, (C_{12}^{\mathrm{L}} P_{\mathrm{L}} + C_{12}^{\mathrm{R}} P_{\mathrm{R}})\, \tilde{\chi}_2(x)\, h(x)\,. \tag{11}$$

Figure 7 refers to the first framework (i.e., allowed $\tilde{\chi}_2^+ \to \tilde{\chi}_1^+ h$ decay) in three different scenarios corresponding to the parameters shown inside the respective plots. The continuous lines show the relative variation $[(\sigma_{\alpha_1} - \sigma_0)/\sigma_0]$ in the total cross section versus a change in the $\alpha_1$ parameter, as defined in (10). The horizontal dashed lines match a variation in the cross section corresponding to the statistical error $\pm\tilde{\sigma}$. Its projection on the $\Delta_{\alpha_1} \equiv \alpha_1 - 1$ axis shows the sensitivity to a change in the $h\tilde{\chi}_1^+\tilde{\chi}_1^-$ coupling in a measurement of the total rate made with an accuracy given by the statistical error (assuming no error on the $h\tilde{\chi}_1^+\tilde{\chi}_2^-$ determination through the $\tilde{\chi}_2^+ \to \tilde{\chi}_1^+ h$ decay). The effect

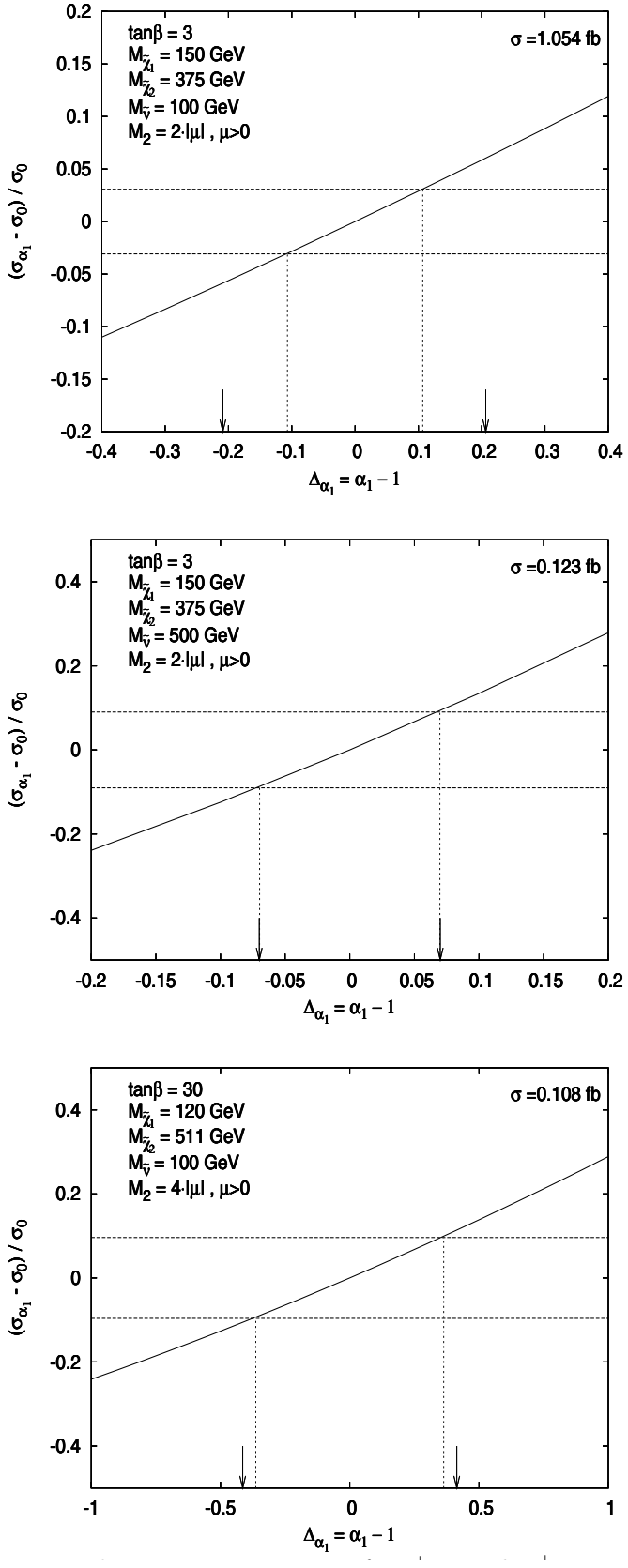


**Fig. 7.** Relative total cross-section variation for $e^+e^- \to h\tilde{\chi}_1^+\tilde{\chi}_1^-$ at $\sqrt{s} = 500\,\text{GeV}$, versus a change in the $\alpha_1$ parameter, as defined in (10), in three different scenarios. Arrows show the effect of a 3% error on the $h\tilde{\chi}_1^+\tilde{\chi}_2^-$ determination

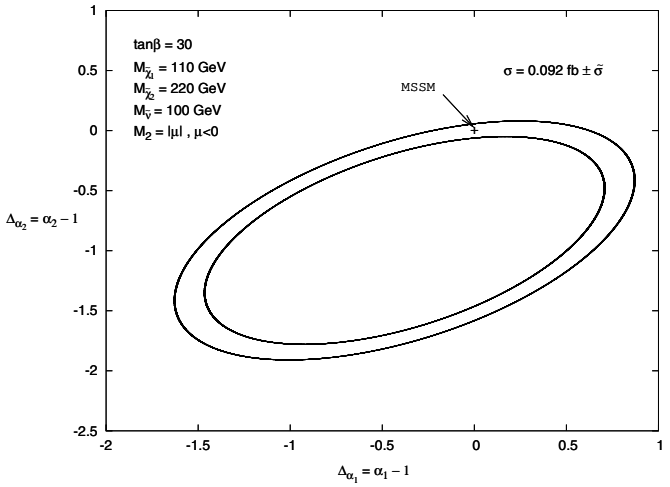


**Fig. 8.** Total cross-section contour plot, corresponding to a variation due to the statistical error $\tilde{\sigma}$, versus a change in both the $h\tilde{\chi}_1^+\tilde{\chi}_1^-$ coupling $\alpha_1$ (as defined in (10)) and the $h\tilde{\chi}_1^+\tilde{\chi}_2^-$ coupling $\alpha_2$ (as defined in (11))

of an error of 3% on the $h\tilde{\chi}_1^+\tilde{\chi}_2^-$ determination is shown by arrows in the same plots. Of course, in scenarios where the amplitudes containing a $\tilde{\chi}_2^+$ are more relevant, this error affects more drastically the final sensitivity to the $h\tilde{\chi}_1^+\tilde{\chi}_1^-$ coupling. For instance, in the second scenario in Fig. 7, the contribution of amplitudes containing a $\tilde{\chi}_2^+$ is negligible, and one obtains a good sensitivity to the $h\tilde{\chi}_1^+\tilde{\chi}_1^-$ coupling even with a moderate total cross section ($\sigma \simeq 0.12\,\text{fb}$). Indeed, in this case, $\alpha_1$ can be determined with an error of about $\pm 7\%$.

Figure 8 refers to the more involved case where the $h\tilde{\chi}_1^+\tilde{\chi}_2^-$ coupling cannot be determined through the $\tilde{\chi}_2^+ \to \tilde{\chi}_1^+ h$ decay, that is not allowed by phase space. In this scenario, we consider the two-dimensional dependence of the total cross section on the variations of both the $h\tilde{\chi}_1^+\tilde{\chi}_1^-$ and the $h\tilde{\chi}_1^+\tilde{\chi}_2^-$ couplings. The area between the two cross-section contour lines corresponds to a change around the MSSM value by the statistical error $\pm\tilde{\sigma}$. In the scenario considered in Fig. 8, one obtains a quite good sensitivity to the $h\tilde{\chi}_1^+\tilde{\chi}_2^-$ coupling (that is better than 10%). At the same time, the sensitivity to the $h\tilde{\chi}_1^+\tilde{\chi}_1^-$ coupling is quite poor.

One can remark that the actual sensitivity of the $e^+e^- \to h\tilde{\chi}_1^+\tilde{\chi}_1^-$ cross section to the $h\tilde{\chi}_1^+\tilde{\chi}_1^-$ coupling can drastically vary with the MSSM parameters. The real potential of the considered process for the Higgs–chargino coupling determination will be set only after the determination of the basic MSSM parameters, following the discovery of supersymmetry.

## 6 Conclusions

In this paper, we analyzed the associated (non-resonant) production of a light Higgs boson and a light-chargino pair in the MSSM, at linear colliders with $\sqrt{s} = 500\,\text{GeV}$.

We computed the total cross section versus MSSM parameters by including the complete set of 13 Feynman

diagrams. Cross sections up to a few fb are found even for chargino masses quite heavier than the present experimental limits.

We discussed a possible strategy to get a first determination of the $h\tilde{\chi}_1^+\tilde{\chi}_1^-$ coupling through the measurement of the total rate for $e^+e^- \to h\tilde{\chi}_1^+\tilde{\chi}_1^-$. The vastly different dynamical characteristics of the various amplitudes contributing to the $e^+e^- \to h\tilde{\chi}_1^+\tilde{\chi}_1^-$ process make in general the assessment of the process potential in studying the light Higgs boson coupling to the charginos extremely model dependent.

We found that, in scenarios where the partial amplitudes that are directly depending on the $h\tilde{\chi}_1^+\tilde{\chi}_1^-$ coupling are dominant, a determination of this coupling within a few percents can be reached on a purely statistical basis, assuming an integrated luminosity of $1\,\mathrm{ab}^{-1}$.

In case the $\tilde{\chi}_2^+ \to \tilde{\chi}_1^+ h$ decay is not allowed by phase space, a measurement of the $h\tilde{\chi}_1^+\tilde{\chi}_2^-$ coupling can also be obtained by the total $e^+e^- \to h\tilde{\chi}_1^+\tilde{\chi}_1^-$ event number, in scenarios where the partial amplitudes depending on the $h\tilde{\chi}_1^+\tilde{\chi}_2^-$ coupling are relevant.

Further analysis of the measurement of the Higgs couplings to charginos, taking into account various systematics and backgrounds, will be needed in order to assess on more solid grounds the potential of the process $e^+e^- \to h\tilde{\chi}_1^+\tilde{\chi}_1^-$.

*Acknowledgements.* We thank S. Heinemeyer, A. Pukhov, and P. Slavich for useful discussions. We also thank D. Choudury for suggesting to us the correlation between the Higgs coupling to the charginos and the ratio $M_2/\mu$.

## Appendix A: Feynman rules

In this appendix we define the couplings, parameters, and constants that have been used in this paper, following the conventions in [4]. In the evaluation of the cross section for the process $e^+e^- \to h\tilde{\chi}_1^+\tilde{\chi}_1^-$, we used the Feynman rules corresponding to the following interaction Lagrangian:

$$\begin{aligned}
\mathcal{L}_{\gamma e^- e^+} &= e\, A^\mu(x)\, \bar{e}(x)\, \gamma_\mu\, e(x)\,, \\
\mathcal{L}_{Z^0 e^- e^+} &= \frac{g}{4\cos\theta_{\mathrm{W}}}\, Z^\mu(x)\, \bar{e}(x)\, \gamma_\mu \\
&\quad \times(1 - 4\sin^2\theta_{\mathrm{W}} - \gamma_5)\, e(x)\,, \\
\mathcal{L}_{\gamma \tilde{\chi}_j^+ \tilde{\chi}_i^-} &= -e\, A^\mu(x)\, \overline{\tilde{\chi}}_i(x)\, \gamma_\mu\, \tilde{\chi}_j(x)\, \delta_{ij}\,, \\
\mathcal{L}_{Z^0 \tilde{\chi}_j^+ \tilde{\chi}_i^-} &= \frac{g}{\cos\theta_{\mathrm{W}}}\, Z^\mu(x)\, \overline{\tilde{\chi}}_i(x)\, \gamma_\mu \\
&\quad \times(O'^{\mathrm{L}}_{ij} P_{\mathrm{L}} + O'^{\mathrm{R}}_{ij} P_{\mathrm{R}})\, \tilde{\chi}_j(x)\,, \\
\mathcal{L}_{h^0 Z^0 Z^0} &= \frac{g\, m_Z}{\cos\theta_{\mathrm{W}}}\, Z^\mu(x)\, Z_\mu(x)\, h(x)\, \sin(\beta-\alpha)\,, \\
\mathcal{L}_{h^0 \tilde{\chi}_j^+ \tilde{\chi}_i^-} &= g\, \overline{\tilde{\chi}}_i(x)\, (C^{\mathrm{L}}_{ij} P_{\mathrm{L}} + C^{\mathrm{R}}_{ij} P_{\mathrm{R}})\, \tilde{\chi}_j(x)\, h(x)\,, \\
\mathcal{L}_{A^0 \tilde{\chi}_j^+ \tilde{\chi}_i^-} &= g\, \overline{\tilde{\chi}}_i(x)\, (C^{A,\mathrm{L}}_{ij} P_{\mathrm{L}} + C^{A,\mathrm{R}}_{ij} P_{\mathrm{R}})\, \tilde{\chi}_j(x)\, A^0(x)\,, \\
\mathcal{L}_{e\tilde{\nu}\tilde{\chi}} &= -g\, \left\{ \bar{e} P_{\mathrm{L}}\, (V_{11}\tilde{\chi}_1^c(x) + V_{21}\tilde{\chi}_2^c(x))\, \tilde{\nu}(x) \right. \\
&\quad \left. + \mathrm{h.c.} \right\}\,, \\
\mathcal{L}_{Z^0 A^0 h^0} &= -\frac{g}{2\cos\theta_{\mathrm{W}}}\, Z_\mu(x) A^0(x) (p^\mu + p'^\mu) \\
&\quad \times \cos(\alpha-\beta)\,, \\
\mathcal{L}_{\tilde{\nu}\tilde{\nu}h^0} &= g \frac{m_W}{2\cos^2\theta_{\mathrm{W}}}\, \sin(\alpha+\beta)\tilde{\nu}(x)\tilde{\nu}(x)h(x)\,,
\end{aligned}$$

where

$$P_{\mathrm{L}} = \frac{1}{2}(1-\gamma_5), \qquad P_{\mathrm{R}} = \frac{1}{2}(1+\gamma_5), \tag{A.12}$$

$$O'^{\mathrm{L}}_{ij} = -V_{i1}V^*_{j1} - \frac{1}{2}V_{i2}V^*_{j2} + \delta_{ij}\sin^2\theta_{\mathrm{W}}, \tag{A.13}$$

$$O'^{\mathrm{R}}_{ij} = -U^*_{i1}V_{j1} - \frac{1}{2}U^*_{i2}U_{j2} + \delta_{ij}\sin^2\theta_{\mathrm{W}} \tag{A.14}$$

and

$$\mathbf{U} = \begin{pmatrix} \cos\phi_- & \sin\phi_- \\ -\sin\phi_- & \cos\phi_- \end{pmatrix}, \tag{A.15}$$

$$\mathbf{V} = \begin{pmatrix} \cos\phi_+ & \sin\phi_+ \\ -\sin\phi_+ & \cos\phi_+ \end{pmatrix}, \tag{A.16}$$

$$\tan(2\phi_-) = 2\sqrt{2} m_W \frac{\mu\sin\beta + M_2\cos\beta}{M_2^2 - \mu^2 - 2m_W^2\cos(2\beta)}, \tag{A.17}$$

$$\tan(2\phi_+) = 2\sqrt{2} m_W \frac{\mu\cos\beta + M_2\sin\beta}{M_2^2 - \mu^2 + 2m_W^2\cos(2\beta)}\,. \tag{A.18}$$

$\mathbf{U}$ are $\mathbf{V}$ are $2\times 2$ unitary matrices that diagonalize the chargino mass matrix $\mathbf{X}$:

$$\mathbf{U}^*\mathbf{X}\mathbf{V}^{-1} = \mathrm{Diag}(m_{\tilde{\chi}_1^\pm}, m_{\tilde{\chi}_2^\pm}), \tag{A.19}$$

$$\begin{aligned} m^2_{\tilde{\chi}_1^\pm}, m^2_{\tilde{\chi}_2^\pm} &= \frac{1}{2}\Big[(|M_2|^2 + |\mu|^2 + 2m_W^2) \\ &\mp \sqrt{(|M_2|^2 + |\mu|^2 + 2m_W^2)^2 - 4|\mu M_2 - m_W^2\sin 2\beta|^2}\Big]\,. \end{aligned} \tag{A.20}$$

Furthermore,

$$C^{\mathrm{L}}_{ij} = \sin\alpha\, Q^*_{ij} - \cos\alpha\, S^*_{ij}, \tag{A.21}$$

$$C^{\mathrm{R}}_{ij} = \sin\alpha\, Q_{ji} - \cos\alpha\, S_{ji}, \tag{A.22}$$

$$C^{A,\mathrm{L}}_{ij} = \sin\beta\, Q^*_{ij} + \cos\beta\, S^*_{ij}, \tag{A.23}$$

$$C^{A,\mathrm{R}}_{ij} = -\sin\beta\, Q_{ji} - \cos\beta\, S_{ji}, \tag{A.24}$$

where $Q_{ij} = \frac{1}{\sqrt{2}}U_{i2}V_{j1}$, $S_{ij} = \frac{1}{\sqrt{2}}U_{i1}V_{j2}$, and

$$\tan\beta = \frac{v_2}{v_1}, \quad \tan(2\alpha) = \tan(2\beta)\left(\frac{m^2_{H^0} + m^2_{h^0}}{m^2_{A^0} + m^2_Z}\right).$$

## Appendix B: Integration of the squared matrix element

In this appendix, we describe the details of the integration of the squared matrix element. In particular, we show the procedure that can be followed in order to get not

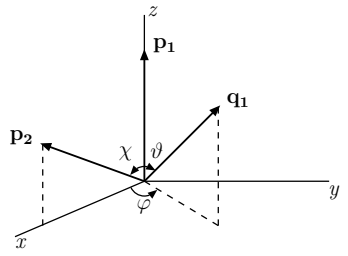


**Fig. 9.** Definition of angular variables in the chargino-pair CM frame

only a completely numerical integration aimed to get total cross sections, but also an analytic expression for the Higgs boson momentum distribution $E_h \frac{\mathrm{d}\sigma}{\mathrm{d}^3\mathbf{h}}$ in the process $e^+e^- \to h\tilde{\chi}_1^+\tilde{\chi}_1^-$. After squaring and summing/averaging over the external spins the square of the matrix element $\mathcal{M} = \sum_{i=1}^{13} \mathcal{M}_i$ obtained from (7) and (8) (we did that with the help of FORM [19]), one can perform two analytic integrations of $|\overline{\mathcal{M}}|^2$ (the squared modulus of $\mathcal{M}$ averaged over the initial particles spin) over the phase-space variables in the following way. Starting from the definition of the momenta

$$e^+(p_1) + e^-(p_2) \longrightarrow \tilde{\chi}_1^+(q_1) + \tilde{\chi}_1^-(q_2) + h^0(h), \quad \text{(B.1)}$$

and

$$\begin{aligned} &p_1 = (E_1, \mathbf{p}_1), \quad p_2 = (E_2, \mathbf{p}_2), \quad q_1 = (E_1', \mathbf{q}_1), \\ &q_2 = (E_2', \mathbf{q}_2), \quad h = (E_h, \mathbf{h}) \,, \end{aligned} \quad \text{(B.2)}$$

the Higgs momentum distribution can be expressed as

$$E_h \frac{\mathrm{d}\sigma}{\mathrm{d}^3\mathbf{h}} = \frac{1}{(2\pi)^5} \int \frac{|\overline{\mathcal{M}}|^2}{16s}\, \delta^4(p_1 + p_2 - q_1 - q_2 - h) \times \frac{\mathrm{d}^3\mathbf{q}_1}{E_1'} \frac{\mathrm{d}^3\mathbf{q}_2}{E_2'} \,, \quad \text{(B.3)}$$

where $s = (p_1 + p_2)^2 = 2(p_1p_2)$.

In order to perform analytically the two non-trivial integrations in (B.3), one can first express $|\overline{\mathcal{M}}|^2$ as a function of the following five independent products of momenta

$$s, \;\; (p_1h), \;\; (p_2h), \;\; (p_1q_1), \;\; (p_2q_1) \,. \quad \text{(B.4)}$$

Then, one can express $(p_1q_1)$ and $(p_2q_1)$ in the chargino-pair CM system (where $\mathbf{q}_1 + \mathbf{q}_2 = \mathbf{0}$) as a function of the angular variables defined in Fig. 9, as follows:

$$(p_1q_1) = \frac{s_1}{4}(1 - \beta\cos\vartheta), \quad \text{(B.5)}$$

$$(p_2q_1) = \frac{s_2}{4}(1 - \beta\cos\vartheta\cos\chi - \beta\sin\vartheta\sin\chi\cos\varphi). \quad \text{(B.6)}$$

where

$$\beta = \sqrt{1 - \frac{4M_1^2}{s + m_h^2 - 2(p_1h) - 2(p_2h)}}, \quad \text{(B.7)}$$

$$\cos\chi = 1 - \frac{2s(s + m_h^2 - 2(p_1h) - 2(p_2h))}{(s - 2(p_1h))(s - 2(p_2h))}, \quad \text{(B.8)}$$

and

$$s_{1,2} = s - 2(p_{1,2}h). \quad \text{(B.9)}$$

Then one can write the differential cross section as

$$E_h \frac{\mathrm{d}\sigma}{\mathrm{d}^3\mathbf{h}} = \frac{\beta}{s(4\pi)^5} \int_{-1}^{1} \mathrm{d}\cos\vartheta \int_0^{2\pi} \mathrm{d}\varphi\, |\overline{\mathcal{M}}|^2 \,, \quad \text{(B.10)}$$

and perform analytically the two angular integrations. The result (which is a quite lengthy expression) is a relativistic invariant function of $(p_1h)$, $(p_2h)$ and $s$.

The total cross section can finally be worked out by integrating numerically the result of (B.10) over the Higgs boson momentum in the $e^+e^-$ CM system (where $\mathbf{p}_1 + \mathbf{p}_2 = 0$),

$$\sigma = 2\pi \int_{{E_h}^{\min}}^{{E_h}^{\max}} \mathrm{d}E_h |\mathbf{h}| \int_{-1}^{1} \mathrm{d}\cos\theta \left[ E_h \frac{\mathrm{d}\sigma}{\mathrm{d}^3\mathbf{h}}((p_1h),(p_2h)) \right]. \quad \text{(B.11)}$$

In (B.11),

$$(p_1h) = \frac{\sqrt{s}}{2}(E_h - |\mathbf{h}|\cos\theta),$$

$$(p_2h) = \frac{\sqrt{s}}{2}(E_h + |\mathbf{h}|\cos\theta),$$

with $|\mathbf{h}| = \sqrt{E_h^2 - m_h^2}$, ${E_h}^{\min} = m_h$, and ${E_h}^{\max} = (s + m_h^2 - 4M_1^2)/(2\sqrt{s})$.

## References


1. E. Accomando et al. [ECFA/DESY LC Physics Working Group Collaboration], Phys. Rept. **299**, 1 (1998) [hep-ph/9705442]; J.A. Aguilar-Saavedra et al. [ECFA/DESY LC Physics Working Group Collaboration], hep-ph/0106315; K. Abe et al. [ACFA Linear Collider Working Group Collaboration], hep-ph/0109166; T. Abe et al. [American Linear Collider Working Group Collaboration], in Proceedings of the APS/DPF/DPB Summer Study on the Future of Particle Physics (Snowmass 2001) edited by N. Graf, hep-ex/0106055; hep-ex/0106056; hep-ex/0106057; hep-ex/0106058
2. J.F. Gunion, H.E. Haber, G.L. Kane, S. Dawson, The Higgs hunter's guide (Addison-Wesley, 1990)
3. H.P. Nilles, Phys. Rept. **110**, 1 (1984)
4. H.E. Haber, G.L. Kane, Phys. Rept. **117**, 75 (1985)
5. R. Barbieri, Riv. Nuovo Cim. **11**, 1 (1988)
6. K.J. Gaemers, G.J. Gounaris, Phys. Lett. B **77**, 379 (1978); A. Djouadi, J. Kalinowski, P.M. Zerwas, Mod. Phys. Lett. A **7**, 1765 (1992); Z. Phys. C **54**, 255 (1992); J.F. Gunion, B. Grzadkowski, X.G. He, Phys. Rev. Lett. **77**, 5172 (1996) [hep-ph/9605326]; H. Baer, S. Dawson, L. Reina, Phys. Rev. D **61**, 013002 (2000) [hep-ph/9906419]; A. Juste, G. Merino, hep-ph/9910301; S. Moretti, Phys. Lett. B **452**, 338 (1999) [hep-ph/9902214]; A. Denner, S. Dittmaier, M. Roth, M.M. Weber, hep-ph/0309274, and references therein
7. G. Belanger, F. Boudjema, T. Kon, V. Lafage, Eur. Phys. J. C **9**, 511 (1999) [hep-ph/9811334]; A. Djouadi, J.L. Kneur, G. Moultaka, Nucl. Phys. B **569**, 53 (2000) [hep-ph/9903218]

8. A. Djouadi, J.L. Kneur, G. Moultaka, Phys. Rev. Lett. **80**, 1830 (1998) [hep-ph/9711244]; A. Dedes, S. Moretti, Phys. Rev. D **60**, 015007 (1999) [hep-ph/9812328]; Eur. Phys. J. C **10**, 515 (1999) [hep-ph/9904491]; G. Belanger, F. Boudjema, K. Sridhar, Nucl. Phys. B **568**, 3 (2000) [hep-ph/9904348]
9. A. Datta, A. Djouadi, J.L. Kneur, Phys. Lett. B **509**, 299 (2001) [hep-ph/0101353]
10. A. Djouadi, J. Kalinowski, P. Ohmann, P.M. Zerwas, Z. Phys. C **74**, 93 (1997) [hep-ph/9605339]; A. Bartl, H. Eberl, K. Hidaka, T. Kon, W. Majerotto, Y. Yamada, Phys. Lett. B **389**, 538 (1996) [hep-ph/9607388]
11. H. Fraas, F. Franke, G. Moortgat-Pick, F. von der Pahlen, A. Wagner, hep-ph/0303044
12. A. Brignole, G. Degrassi, P. Slavich, F. Zwirner, Nucl. Phys. B **631**, 195 (2002) [hep-ph/0112177]; B **643**, 79 (2002) [hep-ph/0206101]
13. LEPSUSYWG, ALEPH, DELPHI, L3 and OPAL experiments, note LEPSUSYWG/01-03.1 and note LEPSUSYWG/02-04.1 (http://lepsusy.web.cern.ch/lepsusy/Welcome.html)
14. M. Baillargeon, F. Boudjema, F. Cuypers, E. Gabrielli, B. Mele, Nucl. Phys. B **424**, 343 (1994) [hep-ph/9307225]
15. B.C. Allanach et al. [Beyond the Standard Model Working Group Collaboration], Les Houches Physics at TeV Colliders 2003 Beyond the Standard Model Working Group: Summary report [hep-ph/0402295]
16. ALEPH, DELPHI, L3, OPAL Collaborations, LEP Higgs Working Group, LHWG Note 2001-4 [ALEPH 2001-057, DELPHI 2001-114, L3 Note 2007, OPAL Technical Note TN699], CERN preprint 2001; OPAL Collaboration, OPAL PN524, CERN preprint 2003
17. R. Barate et al. [ALEPH, DELPHI, L3, OPAL Collaborations, LEP Working Group for Higgs boson searches], Phys. Lett. B **565**, 61 (2003) [hep-ex/0306033]
18. S. Heinemeyer, W. Hollik, G. Weiglein, FeynHiggsFast: A program for a fast calculation of masses and mixing angles in the Higgs sector of the MSSM, hep-ph/0002213
19. J.A.M. Vermaseren, Symbolic manipulation with FORM, (CAN (Computer Algebra Nederland), Kruislaan 413, 1098 SJ Amsterdam, the Netherlands, 1991), ISBN 90-74116-01-9
20. A. Pukhov et al., CompHEP: A package for evaluation of Feynman diagrams and integration over multi-particle phase space. User's manual for version 33, hep-ph/9908288; A. Semenov, Nucl. Instrum. Meth. A **502**, 558 (2003) [hep-ph/0205020]